Structural basis for the specific inhibition of protein kinase G, a virulence factor of *Mycobacterium tuberculosis*

Nicole Scherr*, Srinivas Honnappa†, Gabriele Kunz*, Philipp Mueller*, Rajesh Jayachandran*, Fritz Winkler†, Jean Pieters*‡, and Michel O. Steinmetz†

*Biozentrum, University of Basel, CH-4056 Basel, Switzerland; and †Biomolecular Research, Structural Biology, Paul Scherrer Insititut, CH-5232 Villigen PSI, Switzerland

Edited by Susan S. Taylor, University of California at San Diego, La Jolla, CA, and approved June 4, 2007 (received for review March 27, 2007)

The pathogenicity of mycobacteria such as *Mycobacterium tuberculosis* is closely associated with their capacity to survive within host macrophages. A crucial virulence factor for intracellular mycobacterial survival is protein kinase G (PknG), a eukaryotic-like serine/threonine protein kinase expressed by pathogenic mycobacteria that blocks the intracellular degradation of mycobacteria in lysosomes. Inhibition of PknG with the highly selective low-molecular-weight inhibitor AX20017 results in mycobacterial transfer to lysosomes and killing of the mycobacteria. Here, we report the 2.4 Å x-ray crystal structure of PknG in complex with AX20017. The unique multidomain topology of PknG reveals a central kinase domain that is flanked by N- and C-terminal rubredoxin and tetratrico-peptide repeat domains, respectively. Directed mutagenesis suggests that the rubredoxin domain functions as a regulator of PknG kinase activity. The structure of PknG-AX20017 further reveals that the inhibitor is buried deep within the adenosine-binding site, targeting an active conformation of the kinase domain. Remarkably, although the topology of the kinase domain is reminiscent of eukaryotic kinases, the AX20017-binding pocket is shaped by a unique set of amino acid side chains that are not found in any human kinase. Directed mutagenesis of the unique set of residues resulted in a drastic loss of the compound's inhibitory potency. Our results explain the specific mode of action of AX20017 and demonstrate that virulence factors highly homologous to host molecules can be successfully targeted to block the proliferation of *M. tuberculosis*.

inhibitor | structure | serine–threonine protein kinases

Mycobacterium tuberculosis continues to be one of the world's deadliest pathogens, causing a prospective burden of one billion newly infected individuals and 36 million casualties within the next 20 years (www.tballiance.org). Despite the existence of effective chemotherapies, no new drugs have come to the market in >40 years. In addition, the rise in drug resistance among *M. tuberculosis* strains is becoming a severe threat to public health, illustrated by the recent emergence of extensively (or extremely) drug-resistant tuberculosis (XDR-TB) that has caused a mortality of >98% (1, 2).

Virulence of pathogenic mycobacteria is related to their capacity to survive for prolonged times within macrophage phagosomes (3, 4). Whereas normally internalized and phagocytosed bacteria are rapidly degraded within phagolysosomes, pathogenic mycobacteria have evolved to block lysosomal delivery (4). One strategy by which pathogenic mycobacteria prevent lysosomal maturation is through the activity of mycobacterial protein kinase G (PknG), a eukaryotic-like serine/threonine protein kinase that is not required for mycobacterial growth *per se* but is essential for survival within host macrophages (5, 6). PknG is one of the 11 serine/threonine protein kinases present in *M. tuberculosis* and the only soluble kinase maintained in the genome of *Mycobacterium leprae* that is believed to have retained the minimal set of genes needed for virulence (7). The presence of domains typically found in proteins from eukaryotic species as well as the finding that PknG is dispensable for *in vitro* growth of *M. tuberculosis* (6, 8) suggests that PknG has arrived in the *M. tuberculosis* genome through horizontal gene transfer and has been maintained as a virulence factor important for mycobacterial survival inside the eukaryotic host (9).

Importantly, mycobacteria overexpressing a kinase-dead mutant of PknG are rapidly transferred to lysosomes and killed, demonstrating that PknG kinase activity is crucial for mycobacterial survival. The fact that PknG is translocated into the host cytosol suggests that compounds aimed at blocking PknG activity do not require transport across the only limited permeable mycobacterial cell wall (5). Together, these findings make PknG an attractive and promising drug target. Indeed, blocking PknG kinase activity by a specific small molecular-weight inhibitor, the tetrahydrobenzothiophene AX20017, results in a rapid transfer of mycobacteria to lysosomes and killing of the intracellularly residing bacilli (3, 5).

Despite the relatively simple structure of AX20017, it inhibits PknG with high specificity. To explore the mechanism for this specificity, we solved the structure of the PknG–AX20017 complex by x-ray crystallography. We found that PknG is a multidomain protein consisting of a rubredoxin, kinase, and tetratricopeptide repeat domain and show that the rubredoxin domain is essential for the activity of PknG. The structure reveals that the inhibitor-binding pocket is shaped by a unique set of amino acid residues that, in combination, is not found in any human kinase. The structural information presented here explains the highly specific mode of action of AX20017 and provides a basis for the rational design of novel compounds aimed at blocking the proliferation of *M. tuberculosis*.

Results and Discussion

Specificity of the PknG inhibitor AX20017. The inhibitory activity of AX20017 against the 11 known mycobacterial kinases revealed that the compound is highly selective for PknG (5). To test the activity of the inhibitor toward eukaryotic kinases, a screen of 28

Author contributions: N.S. and S.H. contributed equally to this work; J.P., and M.O.S. designed research; N.S., S.H., G.K., P.M., and R.J. performed research; N.S., S.H., G.K., F.W., J.P., and M.O.S. analyzed data; and J.P. and M.O.S. wrote the paper.

The authors declare no conflict of interest.

This article is a PNAS Direct Submission.

Abbreviations: PknG, protein kinase G; TPR, tetratricopeptide repeat.

Data deposition: The atomic coordinates have been deposited in the Protein Data Bank, www.pdb.org (PDB ID code 2PZI).

‡To whom correspondence should be addressed at: Klingelbergstrasse 50, CH-4056 Basel, Switzerland. E-mail: jean.pieters@unibas.ch.

This article contains supporting information online at www.pnas.org/cgi/content/full/0702842104/DC1.

© 2007 by The National Academy of Sciences of the USA

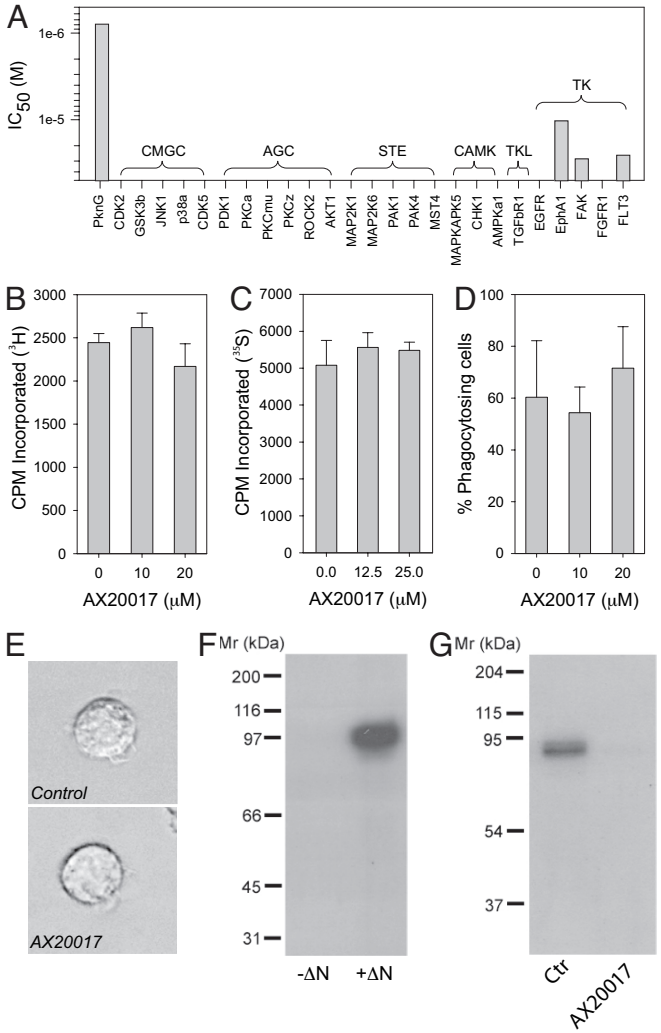

Fig. 1. Specificity of the PknG inhibitor AX20017. (*A*) IC50 determination of AX20017 in an *in vitro* kinase assay screen consisting of PknG and 28 archetypical human kinases originating from six major kinase groups (indicated). (*B*) Macrophage proliferation in the presence and absence of AX20017. (*C*) Protein translation in macrophages left untreated or treated with AX20017. (*D*) Phagocytosis of latex beads (3 μm, 2 h) in the absence or presence of AX20017. Displayed is the percentage of phagocytosing cells (n = 30–50) ± SD. (*E*) J774 cells were left untreated (control) or incubated with 20 μM AX20017, treated with PMA, and observed by video microscopy. (*F* and *G*) *In vitro* kinase assay of PknGΔN (ΔN; 0.5 μg) in the absence (*F* and *G*) or presence (*G*) of 63 μM AX20017. The PknG-K181M kinase-dead mutant was used as a substrate. Reaction mixtures were analyzed after separation by 10% SDS/PAGE by autoradiography. Mr, relative molecular weight.

different archetypical human kinases originating from six major protein kinase groups (10) was set up. The data shown in Fig. 1*A* demonstrate that AX20017 did not affect the human kinases, whereas the activity of PknG was effectively inhibited.

To analyze whether AX20017 interferes with kinase-dependent processes within the macrophage host cell, macrophages were left untreated or incubated with AX20017 and analyzed for their capacity to proliferate, synthesize proteins, and phagocytose, activities that are known to critically depend on host kinase activity (11–13). As shown in Fig. 1 *B–D*, none of these cellular processes were affected by AX20017. Furthermore, video microscopy revealed that the presence of AX20017 did not affect cellular morphology, membrane ruffling, or macropinocytosis [see Fig. 1*E* and supporting information (SI) Movies 1 and 2]. Taken together, these results demonstrate that AX20017 is a highly specific inhibitor of PknG.

Table 1. Crystallographic data and refinement statistics

	Native	Mercury (at λ peak)
Wavelength, Å	1.008503	1.008503
Space group	P65	P65
Resolution, Å	2.4	3.1
Unit cell, *a*, *b*, and *c*, Å	122.6, 122.6 and 243.7	122.4, 122.4 and 241.5
No. of observed reflections	908,852	283,571
No. of unique reflections	80,540	73,241
R_{sym}*, %	7.3 (80.1)†	6.4 (76.0)†
I/σ (I)	20.1 (3.4)†	13.6 (2.1)†
Completeness, %	99.9 (100)†	99.7 (99.6)†
Phasing power (centric/acentric)‡	0.56/0.84	
R_{Cullis} (centric/acentric)§	0.92/0.86	
Figure-of-merit (centric/acentric)¶	0.12/0.14	
No. of refined atoms		
Proteins	9,973	
Water	299	
Ligand/ion	72/3	
R-factor/free *R*-factor‖	0.18/0.23	
R.m.s.d. bond lengths/bond angles**	0.011/1.4	

*$R_{sym} = \Sigma_h\Sigma_i|I_i(h) - \langle I(h)\rangle|/\Sigma_h\Sigma_i I_i(h)$, where $I_i(h)$ and $\langle I(h)\rangle$ are the ith and mean measurement of the intensity of reflection h.

†Figures in parentheses indicate the values for the outer shell of the data.

‡Phasing power $= \Sigma F_H^{calc}/\Sigma|F_{PH}^{obs} - F_{PH}^{calc}|$, where F_H^{calc} is the calculated heavy atom amplitude and F_{PH}^{obs} and F_{PH}^{calc} are the observed and calculated heavy-atom derivative structure factor amplitudes, respectively.

§$R_{Cullis} = \Sigma\,|F_{PH}^{obs} \pm F_P^{obs}| - |F_H^{calc}|/|\Sigma\,|F_{PH}^{obs} - F_P^{obs}|$, where F_{PH}^{obs} is the observed heavy-atom derivative structure factor amplitude, F_P^{obs} is the observed native structure factor amplitude, and F_H^{calc} is the calculated heavy atom amplitude.

¶Figure-of-merit $= \alpha\,|\int\nolimits_\alpha P(\alpha)\exp(i\alpha)d_\alpha/\int\nolimits_\alpha P(\alpha)d_\alpha|$, with α ranging from 0 to 2π.

‖$R = \Sigma\,|F_P^{obs} - F_P^{calc}|/\Sigma\,F_P^{obs}$, where F_P^{obs} and F_P^{calc} are the observed and calculated structure factor amplitudes, respectively.

**R.m.s.d., root-mean-square-deviation from the parameter set for ideal stereochemistry (28).

Structural Analysis of PknG. To define the structural basis of the high specificity of AX20017 for PknG, the crystal structure of the PknG–AX20017 complex was determined by x-ray crystallography. Full-length PknG expressed in bacteria was found to be unstable and yielded only poorly diffracting crystals. Limited proteolysis experiments revealed the formation of a stable protein fragment that lacked the first 73 residues (denoted PknGΔN; SI Fig. 4). In contrast to the full-length protein, the PknGΔN deletion mutant was highly soluble and stable. Furthermore, its kinase activity could be fully inhibited by AX20017 (Fig. 1 *F* and *G*). For the following structural analysis, PknG lacking the first 73 residues was used.

PknG in complex with AX20017 (see Fig. 2*B* for chemical structure) yielded well diffracting crystals that were used to solve the structure at 2.4-Å resolution by single isomorphous replacement anomalous scattering (Table 1). As shown in Fig. 2*A*, the asymmetric unit of the crystal contains two copies of the complex that are related by a noncrystallographic 2-fold (rmsd for 571 backbone atoms equals 0.8 Å). PknG consists of three distinct structural domains whose combination to our best knowledge is not found in any other protein kinase. The C-terminal half of PknG contains a tetratricopeptide repeat (TPR) (14) and assumes a characteristic extended and curved superhelical fold (Fig. 2*A*). This domain interacts with the tip of the C-terminal lobe of the PknG kinase domain. It forms an

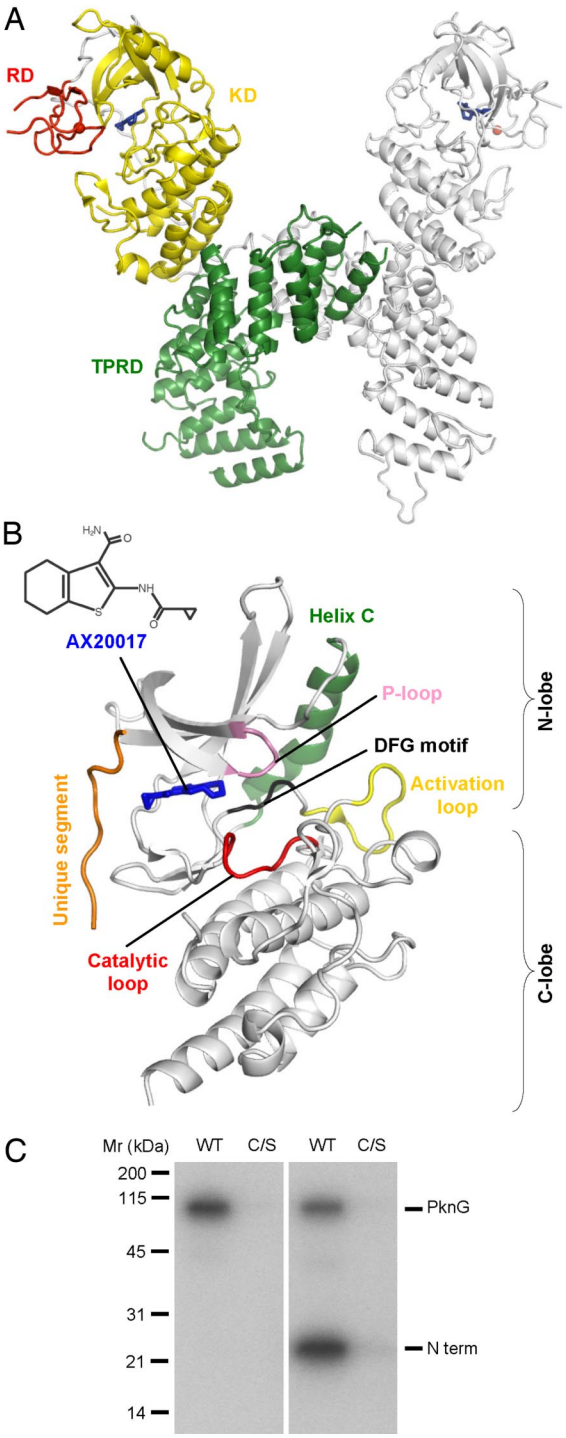

Fig. 2. X-ray crystal structure of the PknG-AX20017 complex. (*A*) Overall fold of the dimeric PknG-AX20017 complex (ribbon representation) as seen in the asymmetric unit of the crystal. The three PknG domains of the left subunit are labeled and depicted in different colors (RD, rubredoxin domain with the bound metal, cadmium in the present structure, depicted as a sphere; KD, kinase domain; TPRD, tetratricopeptide repeat-containing domain). (*B*) Topology of the PknG kinase domain (ribbon representation). Characteristic active site secondary structure elements conserved in protein kinases are indicated in different colors and labeled accordingly. The chemical structure of AX20017 is indicated. In *A* and *B*, the AX20017 molecule is shown in blue sticks representation. (*C*) *In vitro* kinase assay of PknG (WT) and PknG-C/S (Cys-106, Cys-109, Cys-128, and Cys-131 mutated to serines). Reaction mixtures were analyzed after 12.5% SDS/PAGE separation by autoradiography. In the right blot, the N-terminal fragment of PknG was included.

extensive intermolecular lateral contact with the TPR domain of the 2-fold related molecule within the asymmetric unit of the crystal consistent with the known function of TPR domains to mediate protein–protein interactions (14); however, the role of the dimer interface for PknG function is currently not known. The N-terminal part contains two iron-binding Cys-X-X-Cys-Gly (X representing any amino acid residue) motifs characteristic of rubredoxins (15). This small globular domain interacts with both the N- and C-terminal lobes of the PknG kinase domain, packing on top of the active site without blocking its access (Fig. 2*A*). Rubredoxins are used as electron donors in electron-transfer reactions predominantly in certain microorganisms and hence could act as regulatory modules (15). To test whether the rubredoxin domain could modulate the activity of PknG, the four critical metal-coordinating cysteines, Cys-106, Cys-109, Cys-128, and Cys-131 were mutated to serines. Remarkably, the resulting mutant PknG, denoted PknG-C/S, was devoid of activity (Fig. 2*C*). This finding suggests that the activity of PknG might be regulated by the redox status of the environment via the rubredoxin domain.

The kinase domain of PknG is sandwiched between the rubredoxin and the TPR domains. As shown in Fig. 2*B*, it adopts the typical two-lobed structure, with a topology reminiscent of serine/threonine protein kinases. Most active-site signature sequence elements adopt conformations that are characteristic of an activated state of protein kinases (16–18). First, the activation loop, which controls catalytic activity in most kinases by switching between different states, is fully ordered and stabilized in an open and extended conformation (SI Fig. 5*A*). The β9 strand preceding the activation loop forms a short antiparallel β-sheet with the β6 strand preceding the catalytic loop, which provides a site for substrate binding in active states of kinases. Although phosphorylation is the most common mechanism for positioning the activation loop [see, for example, PknB; (19, 20)] it is not phosphorylated in the PknG-AX20017 structure. The absence of an arginine (R) immediately preceding the invariant catalytic aspartate (D) of the catalytic loop (SI Fig. 6*B*) classifies PknG as the unique mycobacterial non-RD kinase (16, 18), explaining the open and extended conformation of the activation loop in the absence of phosphorylation. Second, the side chains of the functionally important and conserved residues such as Asp-276 and Asn-281 of the catalytic loop and Asp-293 of the highly conserved Asp-Phe-Gly motif (denoted DFG) are positioned and adopt conformations similar to their counterparts, Asp-166, Asn-171, and Asp-184 in the active structural state of protein kinase A (PKA) (ref. 21; and see SI Fig. 5 *B* and *C*). Likewise, Lys-181 of PknG is positioned as Lys-72 in the active PKA conformation. However, the ionic interaction observed in PKA between Lys-72 and Glu-91 (Glu-198 in PknG), which is located on the αC helix, is not present in PknG due to a tilted and rotated orientation of this α-helix (SI Fig. 5*D*). The orientation of the αC helix in the present PknG-AX20017 crystal structure appears to be required to avoid a steric clash with the C-terminal part of the activation loop.

Structure of the AX20017-Binding Pocket. As shown in Fig. 2*B*, the AX20017 inhibitor is bound deep within a narrow pocket formed by the interlobe cleft of the kinase domain and a unique peptide segment originating from the N terminus of PknG (residues Pro-85-Met-94). Accessible surface area calculations revealed that 90% of the molecular surface of AX20017 is buried within the kinase domain. A set of 15 residues originating from both the kinase lobes and the unique N-terminal segment of PknG make extensive polar and nonpolar contacts with the inhibitor (Fig. 3*A*). The almost planar tetrahydrobenzothiophene moiety of the inhibitor occupies the conserved hydrophobic pocket that otherwise binds the adenine base of ATP. The main chain Glu-233:O and Val-235:NH of PknG form hydrogen bonds to the

MICROBIOLOGY

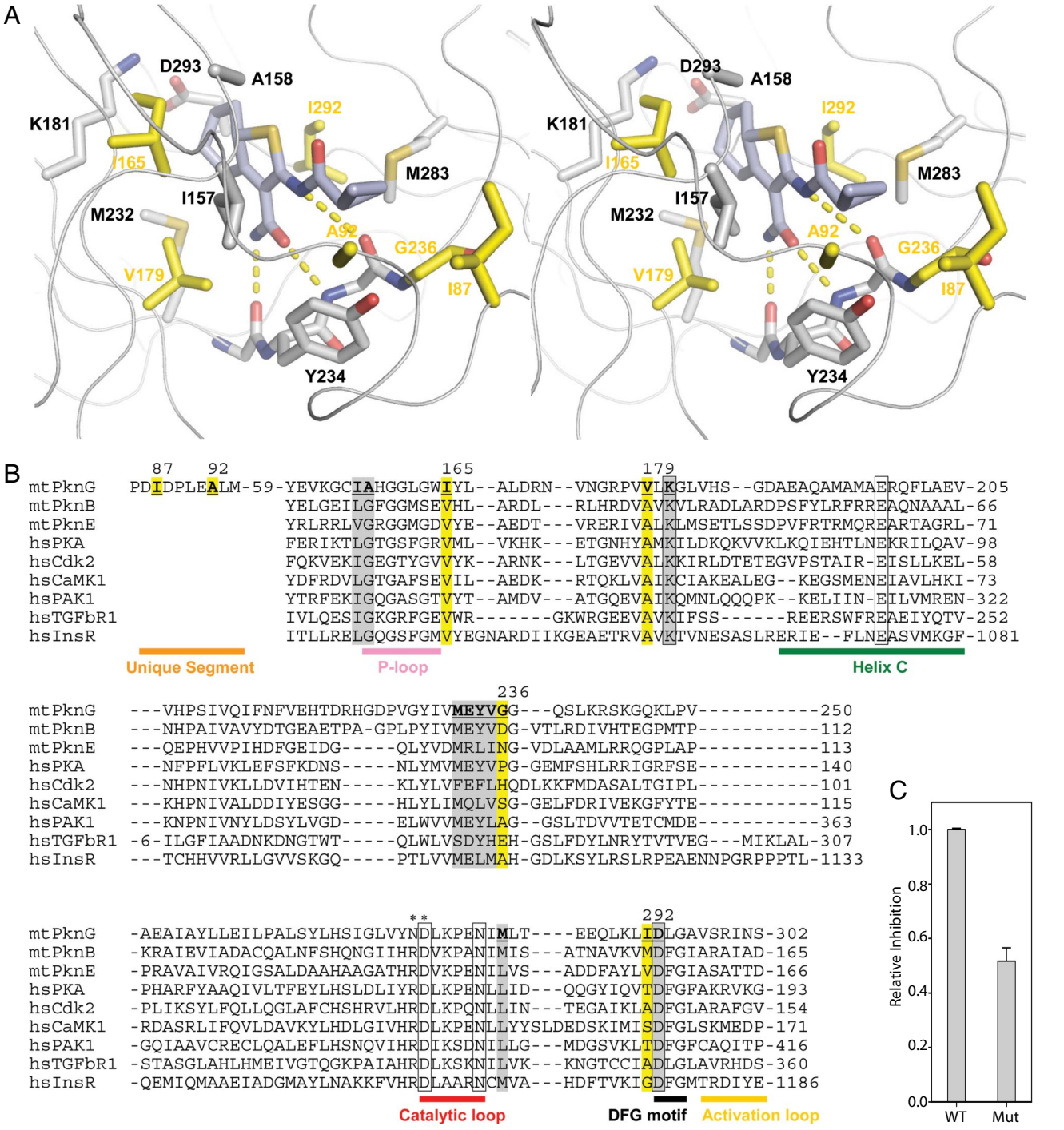

Fig. 3. Binding mode of PknG-AX20017. (*A*) Stereoview of the PknG (gray ribbon and carbon atoms) –AX20017 (light blue carbon atoms) binding site. Interacting residues of PknG are shown in stick representation. Residue side chains, which, in combination, are unique to PknG, are highlighted by yellow carbon atoms. Hydrogen bonds are indicated as dashes. Oxygen, nitrogen, and sulfur atoms are colored in red, blue, and dark yellow, respectively. (*B*) Structure-based sequence alignment of three selected *M. tuberculosis* (8) and six human kinase domains originating from six major kinase groups (10). Selected secondary structure elements of kinase domains are indicated below the alignment. The 15 AX20017-interacting residues of PknG and their identity in homologues are indicated in gray (for variable residues) and yellow (for residues that, in combination, are unique to PknG; residue numbers shown above the sequence correspond to the PknG sequence). Highly conserved catalytic-site residues of protein kinases are indicated by boxes. Asterisks highlight the RD dipeptide motif preceding the catalytic loop. Species identifiers are: mt, *M. tuberculosis*; hs, *Homo sapiens*. UniProtKB/Swiss-Prot and Protein Data Bank accession numbers, respectively, are as follows: PknG (protein kinase G), P65728, 2PZI; PknB (protein kinase B), P0A5S4, 1O6Y; PknE (protein kinase E), P72001, 2H34; PKA (cAMP-dependent protein kinase, AGC group), P17612, 1ATP; Cdk2 (cell division protein kinase 2, CMGC group), P24941, 2BHE; CaMK1 (Calcium/calmodulin-dependent protein kinase type 1, CAMK group), Q14012, 1A06; PAK1 (Serine/threonine-protein kinase PAK 1, STE group), Q13153, 1F3M; TgFβR1 (TGF-β receptor type-1, TKL group), P36897, 1B6C; IRK (insulin receptor, TK group), P06213, 1IRK. (*C*) Inhibitory activity of AX20017 (25 μM) on PknG-I87S/A92S (Mut; 0.5 μg) and comparison with wild-type PknG (WT). Reaction mixtures were analyzed after separation on 12.5% SDS/PAGE by autoradiography.

primary amido substituent of the thiophene ring of the inhibitor, reminiscent of the ones made to the adenosine moiety of ATP (21). An additional hydrogen bond is formed between Val-235:O and the secondary amido group substituent of the thiophene ring. This hydrogen-bonding network places the tetrahydrobenzothiophene moiety of the inhibitor such that van der Waals contacts are made with the side chains of Ala-158, Ile-165, Val-179, Lys-181, Met-232, Ile-292, and Asp-293 of PknG. Apart from the conserved ATP site, the cyclopropyl ring of AX20017 exploits an additional hydrophobic pocket of PknG, which is less homologous among protein kinases. As illustrated in Figs. 2*B* and 3*A*, this moiety of the inhibitor packs against the side chains of Ile-87, Ala-92 of the unique N-terminal segment of PknG, and Ile-157, Tyr-234, Gly-236, and Met-283 of the kinase domain.

Together, these findings show that AX20017 targets both the residues shaping the conserved ATP site and less conserved residues and PknG-specific structural elements adjacent to the ATP site. The remarkable surface complementarities between the PknG kinase domain and inhibitor interfaces (SI Fig. 6) demonstrate that AX20017 exploits the shape and chemical nature of the PknG-binding pocket in a nearly optimal fashion. Sequence comparison of the 11 known *M. tuberculosis* serine/threonine protein kinases (7) revealed that the identities of four inhibitor contacting residues from the conserved kinase domain are specific to PknG (Fig. 3*B*). Sequence analysis of 491 human protein kinases (10) reveals that the frequencies of occurrence of these four individual inhibitor-contacting residues of the ATP site, Ile-165, Val-179, Gly-236, and Ile-292, are 0.037, 0.065, 0.088, and 0.077, respectively. In combination, these four residues are not observed in any human kinase. This finding is illustrated in Fig. 3*B*, which shows a sequence alignment of selected *M. tuberculosis* and human kinase domains originating from six major protein kinase groups (10). Together with the two additional inhibitor contacting residues, Ile-87 and Ala-92, which are unique to PknG, this sequence-to-structure analysis provides a basis for explaining the high specificity of AX20017 for PknG. The precise combination of residues, together with the conformational plasticity of specific structural elements of the PknG kinase domain, appear to generate a uniquely shaped binding pocket for AX20017 not occurring in any other protein kinase. To experimentally test the importance of the two unique PknG inhibitor contacting residues Ile-87 and Ala-92 for AX20017 binding, these residues were both mutated to serines (denoted PknG-I87S/A92S). As shown in Fig. 3*C*, the double mutation resulted in a >50% loss in the inhibitory capacity of AX20017, indicating that the unique N-terminal segment of PknG is important for AX20017 binding.

Implications. Understanding of the virulence factors of pathogenic mycobacteria at the atomic level is required for the development of novel and effective therapeutics for the treatment of diseases caused by these microbes (22, 23). The eukaryotic-like serine/threonine protein kinase PknG plays a crucial role in the survival mechanism of pathogenic mycobacteria, because genetic deletion or chemical inhibition of PknG is sufficient to kill intracellularly residing bacteria (5). Target selection and inhibitor selectivity is of utmost importance because chemical inhibition of a microbial kinase that is highly homologous to its eukaryotic counterparts poses potential risks Since essential host signal transduction pathways may be affected as well (23, 24). The crystal structure of PknG in complex with AX20017 provides insight into how high specificity for blocking a prominent kinase target can be achieved without compromising homologous kinases.

The structural information presented here offers a basis for the rational design of new compounds aimed at blocking the proliferation of *M. tuberculosis*. One promising option to further improve the affinity, selectivity, and potency of AX20017 is to systematically explore modifications of the cyclopropyl ring because this part of the inhibitor does not appear to fully exploit its binding capacity to the unique N-terminal sequence of PknG. In this context, the finding that a small compound such as AX20017 targets an active conformation of PknG may have prospective rewards as the active conformation requires a high degree of structural conservation and the inhibitory mode of action is likely to be less tolerant for the development of resistant mutations (24).

One of the roadblocks in controlling tuberculosis relates to the ability of *M. tuberculosis* to modulate the macrophage innate antimicrobial response, making its host permissive for mycobacterial survival and growth. Because blocking PknG reverts the macrophage into a degradative environment in which mycobacteria are efficiently cleared, the results described here open the possibility of developing a novel class of compounds that is desperately needed with respect to the global tuberculosis epidemic.

Materials and Methods

Cellular Assays. Protein synthesis was analyzed by labeling J774 cells as described (25, 26) by using 0.4 μCi (1 Ci = 37 GBq) of [^{35}S]methione and [^{35}S]cysteine (PerkinElmer, Wellesley, MA) in the continued presence of AX20017 for 9 h. Cells were lysed, and TCA precipitable counts were determined by scintillation counting. Phagocytosis was analyzed after incubation of J774 cells for 30 min in the presence of the indicated concentration of AX20017, followed by incubating the cells for 2 h with latex beads (3-μm diameter; Polysciences, Warrington, PA) at a ratio of 10:1 beads/cells in the continued presence of the inhibitor, followed by fixation in 3% paraformaldehyde as described (27). Cells were observed with a Axiophot (Zeiss, Thornwood, NY) using a ×63 objective. Proliferation of J774 cells was analyzed by incorporation of tritiated thymidine (0.1 μCi) for 12 h as described (28) of cells that had been incubated for 48 h in the absence or presence of the indicated reagents. Video microscopy was done by using a Zeiss Axiovert 100TV and processed by using Openlab software (29).

Limited Proteolysis. PknG [10 mg/ml, in 20 mM Tris (pH 7.5), 75 mM NaCl, and 10% glycerol] was stored at 4°C. To analyze proteolysis, aliquots were taken at different time points and separated by 7.5% SDS/PAGE. Western blotting was performed with antibodies directed against the N- and C-terminal part of PknG. To identify the degradation product, PknG analyzed by gel filtration and SDS/PAGE (10%) was electroblotted onto a PVDF membrane. The different PknG degradation products were excised and subjected to sequence analysis by Edman degradation.

Cloning and Expression. Construction of the bacterial PknG and PknG-K181M expression vectors are described (5). PknGΔN (residues 74–750) and PknG-Nterm (residues 1–147) were amplified by PCR and cloned into pET15b (Novagen, San Diego, CA). The cDNAs encoding PknG-I87S/A92S and the quadruple mutant PknG-C/S (Cys-106, Cys-109, Cys-128, and Cys-131 mutated to serines) were constructed by using the QuikChange Site-Directed Mutagenesis kit (Stratagene, La Jolla, CA). The introduced changes were verified by DNA sequence analysis.

Expression and purification of His-tagged PknG and PknG-K181M was carried out as described (5). For expression of PknGΔN, PknG-Nterm, PknG-I87S/A92S, and PknG-C/S, BL21(DE3) cells were transformed and grown in LB medium containing 100 μg of ampicillin ml^{-1} at 37°C until OD_{600} = 0.5, induced with 0.1 mM isopropyl-β-D-thiogalactopyranosid and incubated for 16 h at 22°C. His-tagged proteins were purified on HiTrap Ni^{2+}-Sepharose chelating and Superdex 200 HiLoad 16/60 columns (Amersham, Piscataway, NJ). Fractions were pooled, and the N-terminal His-tag of PknGΔN was removed by

adding 2 units of thrombin per milligram of protein and 4 mM $CaCl_2$. The protein sample was incubated for 16 h at room temperature and applied to a 1-ml HisTrap HP column (GE Healthcare, Piscataway, NJ) to remove the His-tag. Thrombin was removed by a subsequent size-exclusion chromatography step on a Superdex 200 HiLoad 16/60 column equilibrated in 20 mM Tris (pH 7.5) and 500 mM NaCl. Fractions containing PknGΔN were pooled and concentrated at 4°C to 8–18 mg/ml.

Protein concentrations were determined by the bicinchoninic acid (BCA) Protein Assay (Pierce, Rockford, IL). The structural integrity and solubility of the two PknG mutants, PknG-I87S/A92S and PknG-C/S, was verified by circular dichroism spectroscopy and size-exclusion chromatography, respectively.

Kinase Assay. *In vitro* phosphorylation by PknG (0.5 μg) was carried out as described (5) in 25 mM Tris (pH 7.5), 2 mM $MnCl_2$, and 0.5 μCi [γ-^{32}P]ATP in the absence or presence of the reagents indicated. To monitor kinase activity of PknGΔN, the protein was combined with equal amounts of the kinase-dead mutant of full-length PknG, PknG-K181M. To analyze kinase activity of PknG-I87S/A92S and PknG-C/S, the PknG-N-terminal fragment of PknG (2 μg) was included. Phosphorylated proteins were separated on 12.5% SDS/PAGE and analyzed by autoradiography or quantitated by PhosphorImage analysis using a STORM 840 Optical Scanner System and ImageQuant (version 5.2, Molecular Dynamics, Sunnyvale, CA).

IC_{50} values were determined by using a radiometric ATP consumptive assay (^{33}PanQinase Activity Assay; ProQinase, Freiburg, Germany). Twelve concentrations of AX20017 in the range from 5×10^{-5} M to 1.5×10^{-10} M were tested in each kinase assay.

Crystallization and Structure Determination. PknGΔN (10 mg/ml) was cocrystallized with AX20017 (135 μM final concentration) by mixing equal volumes of the complex with the reservoir solution (each 2 μl) by using the sitting-drop method at 20°C. The crystals grew within 1 day using a reservoir solution containing 100 mM sodium citrate at pH 5.5, 1 M $(NH_4)_2HPO_4$, 200 mM NaCl and 10 mM $CdCl_2$. Data sets were collected at the Swiss Light Source (Villigen PSI, Switzerland) protein beam line X10SA on an MAR CCD detector. All x-ray diffraction data were collected at 100 K. A total of 360 and 240 rotation images of 0.5° were recorded for native and derivative crystals, respectively.

The structure of the PknGΔN-AX20017 complex was solved by single isomorphous replacement with anomalous scattering (SIRAS) using a mercury derivative obtained by overnight soaks of crystals in the presence of 0.5 mM thiomersal. Iterative rounds of model building and maximum-likelihood refinement resulted in a complete 2.4-Å resolution model for the PknGΔN–AX20017 complex. The final model converged at an R/R_{free} of 0.18/0.22 with very good stereochemistry. Data sets and refinement statistics are given in Table 1.

Figures were prepared with the program PyMOL (De-Lano Scientific, San Carlos, CA, www.pymol.org). Solvent-accessible area calculations were carried out with the program NACCESS (http://wolf.bms.umist.ac.uk/naccess).

Sequence Analysis. To calculate the frequency of occurrence of the four individual AX20017-contacting residues, Ile-165, Val-179, Gly-236, and Ile-292 of PknG, an alignment of 491 human kinases was used as a reference (10). The corresponding positions of the four residues within the alignment was corroborated by superimposing the x-ray structure of PknG with the ones of PKA (PDB ID 1ATP), (PDB ID 2BHE), CaMK1 (PDB ID 1A06), PAK1 (PDB ID 1F3M), TgFβR1 (PDB ID 1B6C), and IRK (PDB ID 1IRK). Identical PknG residues in the alignment were counted and divided by 491 to obtain the frequency of occurrence.

We thank Drs. T. Tomizaki from the Swiss Light Source and D. Kostrewa for excellent assistance with the x-ray data collection and processing, respectively, Axxima Pharmaceuticals for providing AX20017, and Dr. Johann Schaller and Urs Kampfer (University of Bern, Bern, Switzerland) for Edman degradation. This work was supported by the Swiss National Science Foundation (J.P. and M.O.S.), the World Health Organization, Olga Mayenfish Stiftung, and the Swiss Life Jubileum Fund (J.P.) and within the framework of the National Center of Competence in Research Structural Biology Program.

1. Anonymous (2006) *Lancet* 368:964.
2. Masjedi MR, Farnia P, Sorooch S, Pooramiri MV, Mansoori SD, Zarifi AZ, Akbarvelayati A, Hoffner S (2006) *Clin Infect Dis* 43:841–847.
3. Nguyen L, Pieters J (2005) *Trends Cell Biol* 15:269–276.
4. Russell DG (2001) *Nat Rev Mol Cell Biol* 2:569–577.
5. Walburger A, Koul A, Ferrari G, Nguyen L, Prescianotto-Baschong C, Huygen K, Klebl B, Thompson C, Bacher G, Pieters J (2004) *Science* 304:1800–1804.
6. Nguyen L, Walburger A, Houben E, Koul A, Muller S, Morbitzer M, Klebl B, Ferrari G, Pieters J (2005) *J Bacteriol* 187:5852–5856.
7. Cole ST, Eiglmeier K, Parkhill J, James KD, Thomson NR, Wheeler PR, Honore N, Garnier T, Churcher C, Harris D, *et al* (2001) *Nature* 409:1007–1011.
8. Av-Gay Y, Everett M (2000) *Trends Microbiol* 8:238–244.
9. Leonard CJ, Aravind L, Koonin EV (1998) *Genome Res* 8:1038–1047.
10. Manning G, Whyte DB, Martinez R, Hunter T, Sudarsanam S (2002) *Science* 298:1912–1934.
11. Xaus J, Comalada M, Valledor AF, Cardo M, Herrero C, Soler C, Lloberas J, Celada A (2001) *Immunobiology* 204:543–550.
12. Hamilton JA (1997) *Mol Reprod Dev* 46:19–23.
13. Vieira OV, Botelho RJ, Grinstein S (2002) *Biochem J* 366:689–704.
14. D'Andrea LD, Regan L (2003) *Trends Biochem Sci* 28:655–662.
15. Sieker LC, Stenkamp RE, LeGall J (1994) *Methods Enzymol* 243:203–216.
16. Johnson LN, Noble ME, Owen DJ (1996) *Cell* 85:149–158.
17. Huse M, Kuriyan J (2002) *Cell* 109:275–282.
18. Nolen B, Taylor S, Ghosh G (2004) *Mol Cell* 15:661–675.
19. Ortiz-Lombardia M, Pompeo F, Boitel B, Alzari PM (2003) *J Biol Chem* 278:13094–13100.
20. Young TA, Delagoutte B, Endrizzi JA, Falick AM, Alber T (2003) *Nat Struct Biol* 10:168–174.
21. Knighton DR, Zheng JH, Ten Eyck LF, Ashford VA, Xuong NH, Taylor SS, Sowadski JM (1991) *Science* 253:407–414.
22. Goulding CW, Apostol M, Anderson DH, Gill HS, Smith CV, Kuo MR, Yang JK, Waldo GS, Suh SW, Chauhan R, *et al.* (2002) *Curr Drug Targets Infect Disord* 2:121–141.
23. Koul A, Herget T, Klebl B, Ullrich A (2004) *Nat Rev Microbiol* 2:189–202.
24. Noble ME, Endicott JA, Johnson LN (2004) *Science* 303:1800–1805.
25. Pieters J, Horstmann H, Bakke O, Griffiths G, Lipp J (1991) *J Cell Biol* 115:1213–1223.
26. Tulp A, Verwoerd D, Dobberstein B, Ploegh HL, Pieters J (1994) *Nature* 369:120–126.
27. Ferrari G, Langen H, Naito M, Pieters J (1999) *Cell* 97:435–447.
28. Jayachandran R, Sundaramurthy V, Combaluzier B, Korf H, Huygen K, Miyazaki T, Albrecht I, Massner J, Pieters J (2007) *Cell*, in press.
29. Gatfield J, Pieters J (2000) *Science* 288:1647–1650.

Corrections

MICROBIOLOGY. For the article "Structural basis for the specific inhibition of protein kinase G, a virulence factor of *Mycobacterium tuberculosis*," by Nicole Scherr, Srinivas Honnappa, Gabriele Kunz, Philipp Mueller, Rajesh Jayachandran, Fritz Winkler, Jean Pieters, and Michel O. Steinmetz, which appeared in issue 29, July 17, 2007, of *Proc Natl Acad Sci USA* (104:12151–12156; first published July 6, 2007; 10.1073/pnas.0702842104), the authors note that, due to a printer's error, Fig. 3*A* was printed too large to be viewed stereoscopically. The corrected figure and its legend appear below.

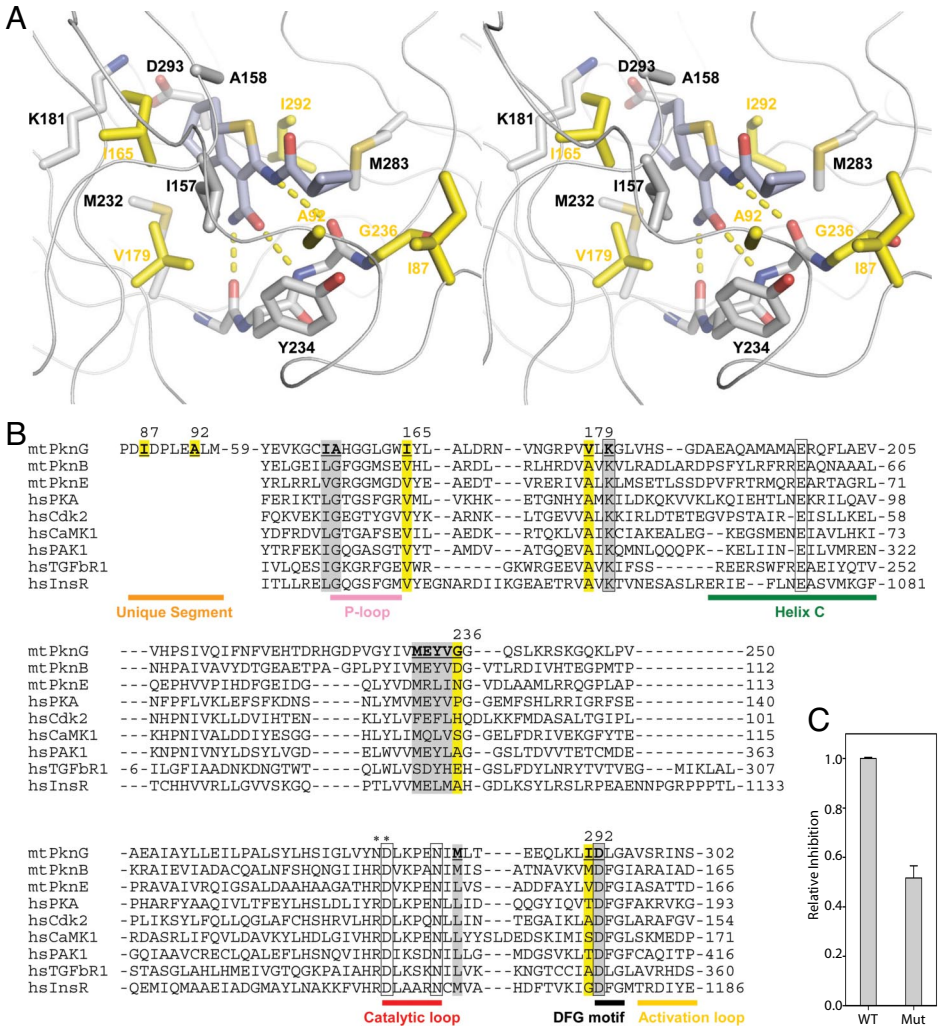

Fig. 3. Binding mode of PknG-AX20017. (*A*) Stereoview of the PknG (gray ribbon and carbon atoms)–AX20017 (light blue carbon atoms) binding site. Interacting residues of PknG are shown in stick representation. Residue side chains, which, in combination, are unique to PknG, are highlighted by yellow carbon atoms. Hydrogen bonds are indicated as dashes. Oxygen, nitrogen, and sulfur atoms are colored in red, blue, and dark yellow, respectively. (*B*) Structure-based sequence alignment of three selected *M. tuberculosis* (8) and six human kinase domains originating from six major kinase groups (10). Selected secondary structure elements of kinase domains are indicated below the alignment. The 15 AX20017-interacting residues of PknG, and their identity in homologues, are indicated in gray (for variable residues) and yellow (for residues that, in combination, are unique to PknG; residue numbers shown above the sequence correspond to the PknG sequence). Highly conserved catalytic-site residues of protein kinases are indicated by boxes. Asterisks highlight the RD dipeptide motif preceding the catalytic loop. Species identifiers are: mt, *M. tuberculosis*; hs, *Homo sapiens*. UniProtKB/Swiss-Prot and Protein Data Bank accession numbers, respectively, are as follows: PknG (protein kinase G), P65728, 2PZI; PknB (protein kinase B), P0A5S4, 1O6Y; PknE (protein kinase E), P72001, 2H34; PKA (cAMP-dependent protein kinase, AGC group), P17612, 1ATP; Cdk2 (cell division protein kinase 2, CMGC group), P24941, 2BHE; CaMK1 (calcium/calmodulin-dependent protein kinase type 1, CAMK group), Q14012, 1A06; PAK 1 (serine/threonine protein kinase PAK 1, STE group), Q13153, 1F3M; TgFβR1 (TGF-β receptor type-1, TKL group), P36897, 1B6C; IRK (insulin receptor, TK group), P06213, 1IRK. (*C*) Inhibitory activity of AX20017 (25 μM) on PknG-I87S/A92S (Mut; 0.5 μg) and comparison with wild-type PknG (WT). Reaction mixtures were analyzed, after separation on 12.5% SDS/PAGE, by autoradiography.

www.pnas.org/cgi/doi/10.1073/pnas.0708192104